

Charge state dynamics of keV ions in solids

R. Holeňák^{1*}, E. Ntemou¹, S. Lohmann² and D. Primetzhofer^{1,2}

¹Materials Physics, Department of Physics and Astronomy, Uppsala University, Box 516, 751 20 Uppsala, Sweden

²Tandem Laboratory, Uppsala University, Box 529, 751 21 Uppsala, Sweden

Abstract

We study charge-exchange dynamics between slow atomic particles and condensed matter revealing a strong dependence of the mean charge state on particle trajectory. Exploiting transmission geometries, single crystalline targets and distributions of the interaction distances obtained in simulations, we show the differences being rooted in the interaction with inner-shell electrons despite the low ion energy. Energy dissipation due to deexcitation of modified inner shell states as well as increased local ionization density due to altered mean charge states aggregate the excessive energy deposition in amorphous targets compared to channeling trajectories and *ab-initio* calculations.

Key-words: Ion transmission, Charge exchange, Reionization, Molecular orbitals

*Corresponding author: radek.holenak@physics.uu.se

Energy deposition by energetic charged particles in matter is governed by the charge state along the path as well as specific charge transfer processes [1]. An accurate description of the charge dynamics of energetic atomic projectiles passing through matter is therefore mandatory for a complete understanding of radiation effects in materials modification or in biological tissues [2,3]. As an a posteriori observable quantity, the integral specific energy loss experienced by projectiles moving through condensed matter has been extensively explored and reasonably understood for swift ions with kinetic energies in the MeV/u range [4]. Our understanding of the detailed nature of energy-loss processes at energies around and below the stopping power maximum has, however, been frequently challenged [5]. In all theoretical efforts on modelling the electronic excitation of matter by energetic, charged projectiles, the necessity of screening due to projectile electrons exemplifies the central role of the projectile charge as well as of charge exchange [6].

The early theoretical description using the free electron gas (FEG) model simplifies the ion-solid interaction into a series of electronic excitations in binary collisions of the projectile with non-local electrons macroscopically manifesting as a friction force [7,8]. Despite the initial successes of the

FEG model in predicting the energy deposition of low-Z projectiles [9–11], an emerging number of experimental works illustrated shortcomings [12,13], in particular due to a strong dependence of electronic excitations on ion-atom distance, the interaction time and implicitly local, dynamic charge-exchange processes. With the advancement in computation power, fully atomistic first-principle calculations of electronic stopping improved the description of the electron dynamics discriminated both in time and space [14]. The models became increasingly capable of predicting the effect of changing electron densities both on the energy loss and fluctuations in the projectile charge [15,16]. Excellent agreement was achieved with experimentally measured stopping of light projectiles [17,18] and heavier projectiles along channeling trajectories [19]. However, the stopping in channeling trajectories is often found up to an order of magnitude lower than the stopping along random trajectories and in amorphous targets [20,21], which represent the most relevant scenario in applications. To reconcile the discrepancy, the excessive energy deposition per unit path for non-channeled trajectories was emulated by models incorporating additional contributions from inner shell electrons [22,23]. Nevertheless, the exact nature of the contribution from inner-shell states of projectile and target atoms to electronic excitations other than treating them as additional valence electrons is difficult to assess [17,24]. Moreover, relevant charge-exchange process like Auger-type transitions are not yet fully incorporated in the current models [25].

In experiments, ion transmission through 2D materials and single crystalline thin membranes was shown as an ideal geometry for accessing energy dissipation and charge-exchange dynamics inside the solid [26,27]. One crucial point of this approach is the ability of a trajectory selection for detected ions which permits linking specific processes with the interaction distances and time scales between projectile and atoms in the target. Notably, electron-exchange dynamics and deexcitation mechanisms were investigated using highly charged ions interacting with down to a single layer of graphene and MoS₂ [28,29]. In a complementary approach, employing thicker films and at near-equilibrium conditions, our recent works reported on an unprecedented increasing relative difference in the energy loss and energy-loss straggling with decreasing velocity between channeled projectiles and those experiencing comparably closer encounters with target nuclei [27,30,31]. These results provided further evidence that additional processes beyond those captured by first-principle calculations, directly and indirectly, contribute to energy dissipation with increasing importance for higher atomic numbers. While the energy transfer occurs in a series of localized events, the measured quantity of energy loss provides only an integral value of such interactions along the trajectory of the projectile and, therefore, no direct access to the underlying mechanism. Nevertheless, other observable quantities like Auger electrons [32–34] or, in particular, the projectile exit charge state [35,36] do carry a memory of only a few (if not one) last interactions.

Charge transfer in the interaction of low-Z particles with only the outermost monolayers of crystalline surfaces and its dependence on interaction distance was addressed in several low-energy ion scattering studies [37–39]. For projectiles with higher Z and noticeably for Ne, the prominent role of the inner shell electrons in determining the energy and the final charge state of the scattered projectile has been investigated in [40–43]. A close collision between the projectile and target atom leading to backscattering was shown to facilitate a sufficient level crossing of the 2p orbitals leading to electron promotion due to the formation of molecular orbitals (MO) followed by ionization [34,44]. The common setting in backscattering experiments, however, can be defined as highly specific with the interaction limited to the outermost atomic layers and small impact parameters resulting in a strong dependence of the observed charge-state distribution on penetration depth [39].

Charge-state distributions of transmitted projectiles and their trajectory dependence were previously investigated at much higher velocities, where interactions can be considered adiabatic [21,45–47]. In this regime, the equilibrium between electron loss and capture shows a dependence on the probed electron densities. Well-channeled projectiles are subjected to reduced charge-exchange probability and thus remain frozen in their initial charge state, which can be higher than the equilibrium charge state established along random trajectories [16,46,47]. In the velocity regime $v \ll v_0$, where a complex dynamic response of the target electronic system to the moving ion is expected, measurements of charge distributions are very scarce for single-crystals like silicon [48], and in general for any other material than carbon studied mainly due to its relevance for time-of-flight measurements [49–51]. However, the observed trajectory dependence of the energy dissipation of ions in solids [20,27,30,52], reemerging at low ion velocities and potentially rooted in local charge-exchange events, is expected to leave a signature in the charge state of the projectile.

In this work, by experiments probing different well-controlled interaction distances and employing projectiles with distinct electronic structures, we show an unprecedented difference in the exit charge-state distributions of slow singly charged projectiles along channeling and pseudo-random trajectories. Significant differences in the exit charge-state distributions were found across the measured energy range in alignment with the previously observed differences in the specific energy loss. Moreover, the mean charge state values for heavier projectiles display a distinct velocity dependence along employed trajectories. Making use of trajectory simulations we correlate the variation in the charge state distribution with the excitation of inner shell electrons.

Experiments were performed with the time-of-flight medium energy ion scattering (TOF-MEIS) setup at Uppsala University [53,54]. A chopped beam of singly charged ions was delivered to the sample within a beam spot size smaller than $1 \times 1 \text{ mm}^2$ and beam angular divergence better than 0.056° . Single-crystalline silicon membranes from Norcada [55] with a nominal thickness of 50 nm and 200 nm were positioned with the 6-axis goniometer in the center of the scattering chamber, 290 mm from

the large solid-angle, position-sensitive detector. Prior to the experiment the samples were dipped in 8% HF and immediately inserted into the vacuum chamber. Transmission MEIS-recoil analysis conducted independently on an identical sample revealed a presence of residual contamination of carbon and oxygen: 4.0 ± 1.1 (10^{15} atoms/cm²) and 1.8 ± 0.6 (10^{15} atoms/cm²), respectively [56]. These values are very comparable to the contamination levels found in the work of Bianconi et al. who adopted the same surface treatment [57]. The base pressure of the chamber was below $2 \cdot 10^{-8}$ mbar.

Different charge states were discriminated with an electrostatic deflection unit positioned at a 0° deflection angle as described in [50]. All charge states are detected simultaneously as narrow bands formed by the slit in front of the deflection plates. The charge-state distributions are obtained by separate integration of the counts within a small rectangular area in the center of each band. The error bars include only the statistical error from the number of counts in the given integration window. Potential further scattering of data might arise from imperfect positioning of the deflector, a change in the flight-time distance due to sample rotation and the complex angular distribution of the transmitted projectiles in random geometry induced by the blocking effect [58]. The sensitivity varies for different trajectories; detection limits for charge fractions of 0.001% and 0.1% were achieved for channeling and random, respectively. The exit velocity of the transmitted projectiles was evaluated from the central neutral charge band in the absence of an electrostatic field. The maximum final deflection angle in the sample considered in the evaluation was 0.2 degrees restraining the detectable trajectories to the straightest ones.

The experimentally derived mean charge ($\langle Z \rangle = \sum n f_n$, where f_n denotes a charge fraction from the measured charge-state distributions) for the He and Ne projectiles transmitted through the Si membrane as a function of their exit velocity is presented in Figure 1. Differences in mean charge values are apparent between channel and random trajectories separating towards lower and higher mean values with respect to the mean charges of He and Ne ions found after transmission through an amorphous carbon membrane in [50] and [59]. Along with our data, the figure features experimental data from Buck et al. [48] for neutral and one plus fractions of He derived from a subsurface signal in backscattering from a Si crystal. In absolute values, the mean charges observed for He are considerably lower compared to the purely theoretical prediction of Bohr and Thomas-Fermi for the mean charge state of He within the solid. A closer agreement is reached with the semiempirical prediction from Grande and Schiwietz [49] despite the limited validity of their formula in the low-velocity regime.

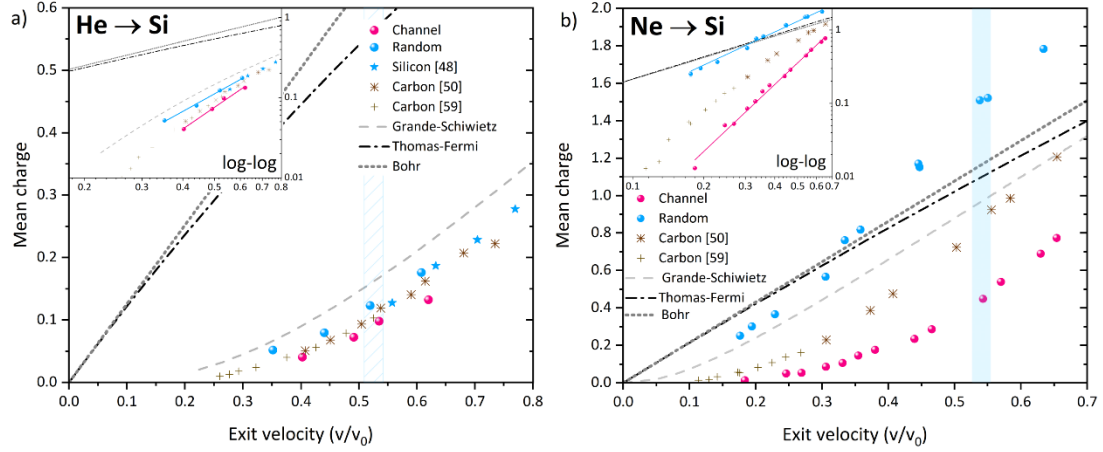


Figure 1 Mean charge state of a) He and b) Ne ions transmitted through 50 nm and 200 nm thick single-crystalline Si membranes along with the mean charge state values for He in Si from [48] and He and Ne in C from [50] and [59]. Experimental data are compared to two theoretical and one semiempirical predictions by Bohr and Thomas-Fermi as well as Grande-Schiwietz, respectively. The insets indicate that different power laws govern the velocity dependence for different trajectory types.

Markedly larger differences are found for the derived mean charge states of Ne for the two different trajectories as compared to the He dataset. The directionality of the separation from the carbon data shows an identical trend as for He but at much larger magnitude. The trends of the mean charge values for random and channeling trajectories follow different power scaling laws (see log-log inset in Fig. 1 b) proportional to $(v/v_0)^{2/3}$ for random and $(v/v_0)^3$ for channeling data. Consequently, the ratio Q_{Ch}/Q_R itself shows a strong velocity dependence ranging from 0.43 at the highest velocities to 0.05 at the lowest, where the mean charge along channeling is approaching 0. The two plotted theoretical predictions largely overestimate the mean charge along channeling trajectories while underestimating the mean charge along random trajectories above the intersection at around 0.3 a.u. The formula by Grande and Schiwietz predicts lower mean charge along random trajectory throughout the explored velocity range.

Figure 2 shows the distribution of individual charge states of He and Ne projectiles for channeling and random trajectories in Si selected in a narrow velocity range between 0.51 a.u. and 0.56 a.u. also marked with blue rectangles in Figure 1. For He, the difference between the two employed trajectories is most pronounced for the He^{2+} fraction. For Ne travelling along random trajectories, the higher ionization states 2^+ , 3^+ , and 4^+ are orders of magnitude more abundant than in channeling geometry. Note that e.g. Ne^{3+} represents more than 15% of the mean value and is comparable to the amount of Ne^0 . Detection of higher charge fractions of Ne was obscured due to the limited sensitivity. Nevertheless, from the shape of the charge state distribution of Ne projectiles along random trajectories, the existence of higher charge fractions than 4^+ can be inferred.

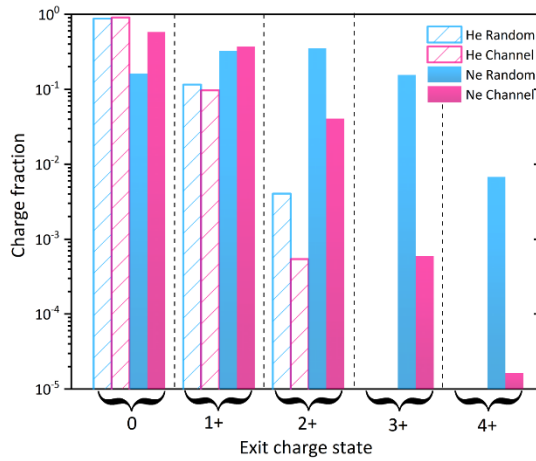


Figure 2 Charge state distributions of He and Ne at exit velocity between 0.51 - 0.56 a.u. The sensitivity of the method for the given system prevents observation of charge fractions higher than 4+ for Ne projectiles.

To understand the origin of the observed charge differences and their implications on the energy-loss processes, critically assessing the influence of the surface of the target including common carbon contaminations is a necessity. Measurements for hydrogen ions emerging from freshly deposited surfaces show that the equilibrium charge-state distributions are determined by the last few (~5) atomic layers [60]. With the charge survival rates for He in carbon with various hybridization states reported in [61,62], the corresponding Auger neutralization rate for sp^3 and sp^2 hybridization is about a factor two and a factor four higher, respectively, than the Auger rates reported in metals [36]. For a He projectile from Figure 2 with a velocity of $\sim 12 \text{ \AA}/\text{fs}$ and the experimentally derived carbon contamination of $\sim 3.5 \text{ \AA}$, the neutralization probability for a singly charged particle in sp^3 carbon can be as high as 70%. For Ne, the charge equilibration process close to the surface appears less effective than for He, resulting in an observation of considerably higher charge state along random trajectories. Furthermore, the fact, that the channeled trajectories end up with a mean charge state well below what has been observed for carbon indicates that projectiles are unlikely to get reionized in the last close encounter with carbon atoms before exiting the membrane. Ergo, due to the surface contamination, we expect, the here observed difference in charge states to be lower than the true equilibrium value in the solid.

Employing computer simulations, we show in the following that even for relatively straight trajectories in transmission geometry, the probed interaction instances are sufficiently small to allow for a frequent effective overlap of atomic orbitals leading to repeated electron promotion and subsequent ionization, explaining the observed discrepancy in charge states for the different trajectories. These processes accompanied by large inelastic energy losses were previously reported only in hard-binary collision in a gaseous medium or with target surfaces [42,63–66]. Recently, we

have demonstrated how transmission experiments can be coupled with MC-BCA calculations to develop a better understanding of complex projectile trajectories [67]. Now, we employ these simulations to determine the distribution of interaction distances along the projectile trajectories for 33 keV He and 180 keV Ne considered in the current experiment. The final distributions of the average number of collisions per trajectory as a function of the collision distance are presented in Figure 3. The figure further features the radial distributions of the electronic density $\rho(R)$ of Si as well as of He and Ne adopted from the stopping power model CasP [68,69]. Critical distances for formations of MO from [40,70] are indicated by arrows labelled R_c . A pronounced difference in the distribution of collision distances is found between random and channeling trajectories, especially in the context of relative overlap between the electronic orbitals with the target atom. The distribution of interaction distances for He and Ne are nonetheless very similar and can be shown to exhibit sufficient crossing of the critical distance over a wide velocity range below v_0 covered in this work. Consequently, the collision-induced charge-exchange processes are expected to contribute to the energy loss even in low-angle collisions effectively decoupling these large electronic loss processes from the large elastic energy transfer observed in low-energy ion backscattering [66]. The electron promotion mechanism as an active energy dissipation channel, nevertheless, will exhibit a velocity dependence correlated with the reduced timescales available for effective electron promotions at high projectile velocities [71].

In the framework of the formation of MO, the reionization of He takes place due to the antibonding interaction of the He 1s level with the target core (2p) levels accessible only in close collisions with target atoms [33,66,70]. The BCA calculation for the random trajectory of 33 keV He in 50 nm Si crystal reveals that the critical distance of $\sim 0.35 \text{ \AA}$ is reached at least a few times (approximately every 30 monolayers). Although these processes are accompanied by direct energy losses [72], the small relative change in abundance of the higher charge fraction between the two trajectories shown in Fig. 2 would indicate that the higher energy loss along random trajectories is to largest extent a consequence of a stronger Coulombic interaction since higher electron densities are probed [73,74] as well as due to an increased effective charge of the projectiles [75]. This interpretation is further corroborated by the measurements of energy-loss straggling that revealed that for He along both trajectories, the energy is transferred predominately via direct electron-hole pair excitations of the target [31]. For the case of Ne, the works of Xu et al. [40] and Gordon et al. [42] reported a critical distance of $\sim 0.6 \text{ \AA}$ below which the promotions in the $4f\sigma$ orbital (correlated to the Ne 2p), but potentially also promotions along other MO become relevant [76–78]. The BCA calculation for random but straight trajectories of 180 keV Ne in a 50 nm silicon crystal reveals that this critical distance is overcome multiple times (approximately every 8 monolayers). The significantly higher frequency of such close collisions compared to He along with a number of possible excitation channels

render electron promotion and subsequent ionization phenomena largely responsible for the observed differences in charge-state distributions between He and Ne ions and inevitably in the total energy losses. Channeling trajectories on the other hand exclusively probe a nearly homogenous electron gas formed by the silicon 3s and 3p electrons for which the FEG approximation could still be appropriate [30]. The observed differences in charge-state distributions between the two geometries are expected to be even more significant if a perfect atomically clean surface was conserved. The shortcoming of the theoretical models in accurately predicting the experimental data is rooted in the unaccounted influence of multi-electron processes requiring a complete modelling of inner shells, meta-stable excited states as well as radiative transitions of the highly excited electronic system of the projectile [49].

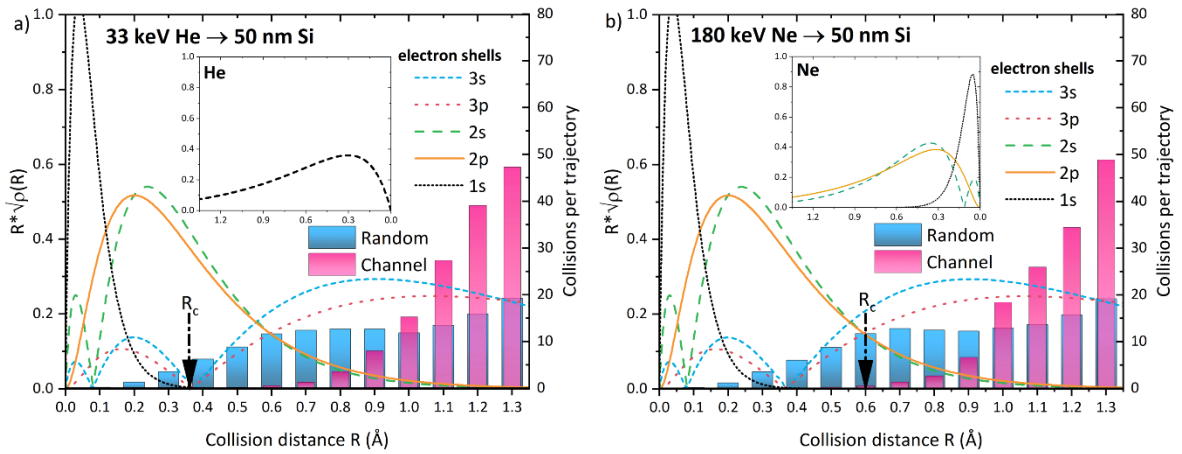


Figure 3 Distribution of probed collisional distances per trajectory of a) 33 keV He ($v = 0.58$ a.u.) and b) 180 keV Ne ($v = 0.57$ a.u.) transmitted through 50 nm silicon membrane for channeling and random orientations collected under scattering angles less than 0.2 degrees. The figure features the radial distribution of electronic densities for individual electron shells of both Si and, as insets, for respective projectiles as well as the critical distances for the formation of MO, R_c [40,70].

The here accessed magnitude of the differences in the final charge-state distribution along with the variation in velocity scaling, especially for Ne, directly illustrates the crucial role of charge exchange in the interaction of keV projectiles with solids. Our results proof that projectile charge and energy loss evolve dynamically along the projectile trajectory and have to be jointly considered to obtain accurate predictions. The present observation is accordingly complementing the observed trajectory dependence of energy loss and energy-loss straggling yielding an explanation in one common framework. The now explicitly shown more frequently occurring ionization along random trajectories corroborates the influence of inner shell electrons participating in the projectile-solid excitation via electron promotion. At the same time, the observed variations in projectile charge state challenge theoretical models in which interactions with a denser electron gas at short interaction distances promote electron capture, i.e. neutralization not ionization. In particular for heavier

projectiles, we show that the specific match of the inner shells with the electronic structure of the solid can drastically change the number of available excitation and energy loss channels and via the altered mean charge state also affect the direct ionization losses. The results obtained here enable therefore a thorough understanding of highly perturbative electron dynamics in solids by correlatively assessing ion charge states and energy loss moments varying atomic number and thus shell structure of projectile and target nuclei. Additional correlation with secondary particles such as electrons emitted from decaying excitation states of ion and target could provide further direct information on the relevant transient electronic states.

Acknowledgements

Accelerator operation is supported by the Swedish Research Council VR-RFI (Contract No. 2019_00191).

References

- [1] P. Sigmund, *Charge-Dependent Electronic Stopping of Swift Nonrelativistic Heavy Ions*, Phys. Rev. A **56**, 3781 (1997).
- [2] B. Schmidt and K. Wetzig, *Ion Beams in Materials Processing and Analysis* (Springer Vienna, Vienna, 2013).
- [3] A. Rucinski, A. Biernacka, and R. Schulte, *Applications of Nanodosimetry in Particle Therapy Planning and Beyond*, Phys. Med. Biol. **66**, 24TR01 (2021).
- [4] P. Sigmund, *Six Decades of Atomic Collisions in Solids*, Nucl. Instruments Methods Phys. Res. Sect. B Beam Interact. with Mater. Atoms **406**, 391 (2017).
- [5] J. I. Juaristi, C. Auth, H. Winter, A. Arnau, K. Eder, D. Semrad, F. Aumayr, P. Bauer, and P. M. Echenique, *Unexpected Behavior of the Stopping of Slow Ions in Ionic Crystals*, Phys. Rev. Lett. **84**, 2124 (2000).
- [6] N. Bohr, *The Penetration of Atomin Particles through Matter*, Dan. Videns. Sels. Mat-Fys. Medd. **28**, (1948).
- [7] P. M. Echenique, R. M. Nieminen, and R. H. Ritchie, *Density Functional Calculation of Stopping Power of an Electron Gas for Slow Ions*, Solid State Commun. **37**, 779 (1981).
- [8] P. M. Echenique, F. Flores, and R. H. Ritchie, *Dynamic Screening of Ions in Condensed Matter*, in *Solid State Physics - Advances in Research and Applications*, Vol. 43 (1990), pp. 229–308.
- [9] J. E. Valdés, G. Martínez Tamayo, G. H. Lantschner, J. C. Eckardt, and N. R. Arista, *Electronic Energy Loss of Low Velocity H+ Beams in Al, Ag, Sb, Au and Bi*, Nucl. Instruments Methods

- Phys. Res. Sect. B Beam Interact. with Mater. Atoms **73**, 313 (1993).
- [10] J. E. Valdés, J. C. Eckardt, G. H. Lantschner, and N. R. Arista, *Energy Loss of Slow Protons in Solids: Deviation from the Proportionality with Projectile Velocity*, Phys. Rev. A **49**, 1083 (1994).
- [11] S. N. Markin, D. Primetzhofer, S. Prusa, M. Brunmayr, G. Kowarik, F. Aumayr, and P. Bauer, *Electronic Interaction of Very Slow Light Ions in Au: Electronic Stopping and Electron Emission*, Phys. Rev. B **78**, 195122 (2008).
- [12] S. N. Markin, D. Primetzhofer, and P. Bauer, *Vanishing Electronic Energy Loss of Very Slow Light Ions in Insulators with Large Band Gaps*, Phys. Rev. Lett. **103**, 1 (2009).
- [13] D. Primetzhofer, S. Rund, D. Roth, D. Goebel, and P. Bauer, *Electronic Excitations of Slow Ions in a Free Electron Gas Metal: Evidence for Charge Exchange Effects*, Phys. Rev. Lett. **107**, 163201 (2011).
- [14] A. Schleife, Y. Kanai, and A. A. Correa, *Accurate Atomistic First-Principles Calculations of Electronic Stopping*, Phys. Rev. B - Condens. Matter Mater. Phys. **91**, 014306 (2015).
- [15] Y.-L. Fu, C.-K. Li, H.-B. Sang, W. Cheng, and F.-S. Zhang, *Electronic Stopping Power under Channeling Conditions for Slow Ions in Ge Using First Principles*, Phys. Rev. A **102**, 012803 (2020).
- [16] C. W. Lee, J. A. Stewart, R. Dingreville, S. M. Foiles, and A. Schleife, *Multiscale Simulations of Electron and Ion Dynamics in Self-Irradiated Silicon*, Phys. Rev. B **102**, 24107 (2020).
- [17] C.-K. Li, J. Xue, and F.-S. Zhang, *Channeling Electronic Stopping Power of Lithium Ions in Diamond: Contribution of Projectile Inner-Shell Electrons*, Phys. Rev. A **106**, 022807 (2022).
- [18] E. Ponomareva, E. Pitthan, R. Holeňák, J. Shams-Latifi, G. P. Kiely, D. Primetzhofer, and A. E. Sand, *Local Electronic Excitations Induced by Low-Velocity Light Ion Stopping in Tungsten*, Phys. Rev. B **109**, 165123 (2024).
- [19] A. Lim, W. M. C. Foulkes, A. P. Horsfield, D. R. Mason, A. Schleife, E. W. Draeger, and A. A. Correa, *Electron Elevator: Excitations across the Band Gap via a Dynamical Gap State*, Phys. Rev. Lett. **116**, 043201 (2016).
- [20] F. H. Eisen, *Channeling of Medium-Mass Ions through Silicon*, Can. J. Phys. **46**, 561 (1968).
- [21] W. Jiang, R. Grötzschel, W. Pilz, B. Schmidt, and W. Möller, *Random and Channeling Stopping Powers and Charge-State Distributions in Silicon for 0.2–1.2 MeV/u Positive Heavy Ions*, Phys. Rev. B **59**, 226 (1999).
- [22] R. Ullah, E. Artacho, and A. A. Correa, *Core Electrons in the Electronic Stopping of Heavy Ions*, Phys. Rev. Lett. **121**, 116401 (2018).
- [23] F. Matias, P. L. Grande, M. Vos, P. Koval, N. E. Koval, and N. R. Arista, *Nonlinear Stopping Effects of Slow Ions in a No-Free-Electron System: Titanium Nitride*, Phys. Rev. A **100**, 30701

- (2019).
- [24] A. Ojanpera, A. V. Krashennikov, and M. Puska, *Electronic Stopping Power from First-Principles Calculations with Account for Core Electron Excitations and Projectile Ionization*, Phys. Rev. B - Condens. Matter Mater. Phys. **89**, 1 (2014).
 - [25] G. Zhou, G. Lu, and O. V. Prezhdo, *Modeling Auger Processes with Nonadiabatic Molecular Dynamics*, Nano Lett. **21**, 756 (2021).
 - [26] R. A. Wilhelm, *The Charge Exchange of Slow Highly Charged Ions at Surfaces Unraveled with Freestanding 2D Materials*, Surf. Sci. Rep. **77**, 100577 (2022).
 - [27] S. Lohmann and D. Primetzhofer, *Disparate Energy Scaling of Trajectory-Dependent Electronic Excitations for Slow Protons and He Ions*, Phys. Rev. Lett. **124**, 096601 (2020).
 - [28] A. Niggas et al., *Ion-Induced Surface Charge Dynamics in Freestanding Monolayers of Graphene and MoS₂ Probed by the Emission of Electrons.*, Phys. Rev. Lett. **129**, 086802 (2022).
 - [29] T. Jahnke, *Interatomic and Intermolecular Coulombic Decay: The Coming of Age Story*, J. Phys. B At. Mol. Opt. Phys. **48**, 082001 (2015).
 - [30] S. Lohmann, R. Holeňák, and D. Primetzhofer, *Trajectory-Dependent Electronic Excitations by Light and Heavy Ions around and below the Bohr Velocity*, Phys. Rev. A **102**, 062803 (2020).
 - [31] S. Lohmann, R. Holeňák, P. L. Grande, and D. Primetzhofer, *Trajectory Dependence of Electronic Energy-Loss Straggling at KeV Ion Energies*, Phys. Rev. B **107**, 085110 (2023).
 - [32] R. A. Baragiola, E. V. Alonso, and A. O. Florio, *Electron Emission from Clean Metal Surfaces Induced by Low-Energy Light Ions*, Phys. Rev. B **19**, 121 (1979).
 - [33] P. Riccardi, A. Sindona, and C. A. Dukes, *Local Charge Exchange of He⁺ Ions at Aluminum Surfaces*, Phys. Lett. A **381**, 1174 (2017).
 - [34] D. Runco and P. Riccardi, *Single versus Double 2p Excitation in Neon Projectiles Scattered from Surfaces*, Phys. Rev. A **104**, 042810 (2021).
 - [35] R. A. Wilhelm, E. Gruber, V. Smejkal, S. Facsko, and F. Aumayr, *Charge-State-Dependent Energy Loss of Slow Ions. I. Experimental Results on the Transmission of Highly Charged Ions*, Phys. Rev. A **93**, 052708 (2016).
 - [36] D. Primetzhofer, S. N. Markin, J. I. Juaristi, E. Taglauer, and P. Bauer, *Crystal Effects in the Neutralization of He⁺ Ions in the Low Energy Ion Scattering Regime*, Phys. Rev. Lett. **100**, 213201 (2008).
 - [37] T. M. Buck, G. H. Wheatley, and L. K. Verheij, *Low-Energy Neon-Ion Scattering and Neutralization on First and Second Layers of a Ni(001) Surface*, Surf. Sci. **90**, 635 (1979).
 - [38] W. Eckstein, V. A. Molchanov, and H. Verbeek, *The Charge States of He and Ne Backscattered from Ni in the Energy Range of 1.5–15 KeV*, Nucl. Instruments Methods **149**, 599 (1978).
 - [39] D. Primetzhofer, M. Spitz, E. Taglauer, and P. Bauer, *Resonant Charge Transfer in Low-Energy*

- Ion Scattering: Information Depth in the Reionization Regime*, Surf. Sci. **605**, 1913 (2011).
- [40] F. Xu, G. Manicò, F. Ascione, A. Bonanno, A. Oliva, and R. A. Baragiola, *Inelastic Energy Loss in Low-Energy Ne⁺ Scattering from a Si Surface*, Phys. Rev. A **57**, 1096 (1998).
- [41] O. Grizzi, E. A. Sánchez, J. E. Gayone, L. Guillemot, V. A. Esaulov, and R. A. Baragiola, *Formation of Autoionizing Ne^{**} in Grazing Collisions with an Al(111) Surface*, Surf. Sci. **469**, 71 (2000).
- [42] M. J. Gordon, J. Mace, and K. P. Giapis, *Charge-Exchange Mechanisms at the Threshold for Inelasticity in Ne⁺ Collisions with Surfaces*, Phys. Rev. A **72**, 012904 (2005).
- [43] J. Mace, M. J. Gordon, and K. P. Giapis, *Evidence of Simultaneous Double-Electron Promotion in F⁺ Collisions with Surfaces*, Phys. Rev. Lett. **97**, 1 (2006).
- [44] M. Barat and W. Lichten, *Extension of the Electron-Promotion Model to Asymmetric Atomic Collisions*, Phys. Rev. A **6**, 211 (1972).
- [45] S. Datz, F. W. Martin, C. D. Moak, B. R. Appleton, and L. B. Bridwell, *Charge-Changing Collisions of Channeled Oxygen Ions in Gold*, Radiat. Eff. **12**, 163 (1972).
- [46] C. D. Moak, S. Datz, B. R. Appleton, J. A. Biggerstaff, M. D. Brown, H. F. Krause, and T. S. Noggle, *Influence of Ionic Charge State on the Stopping Power of 27.8- and 40-MeV Oxygen Ions in the [011] Channel of Silver*, Phys. Rev. B **10**, 2681 (1974).
- [47] G. Bentini, E. Albertazzi, M. Bianconi, R. Lotti, and G. Lulli, *Charge States Distribution of 3350 KeV He Ions Channeled in Silicon*, Nucl. Instruments Methods Phys. Res. Sect. B Beam Interact. with Mater. Atoms **193**, 113 (2002).
- [48] T. M. Buck, G. H. Wheatley, and L. C. Feldman, *Charge States of 25–150 KeV H and 4He Backscattered from Solid Surfaces*, Surf. Sci. **35**, 345 (1973).
- [49] G. Schiwietz and P. Grande, *Improved Charge-State Formulas*, Nucl. Instruments Methods Phys. Res. Sect. B Beam Interact. with Mater. Atoms **175–177**, 125 (2001).
- [50] R. Holeňák, S. Lohmann, F. Sekula, and D. Primetzhofer, *Simultaneous Assessment of Energy, Charge State and Angular Distribution for Medium Energy Ions Interacting with Ultra-Thin Self-Supporting Targets: A Time-of-Flight Approach*, Vacuum **185**, 109988 (2021).
- [51] R. Kallenbach, M. Gonin, P. Bochsler, and A. Bürgi, *Charge Exchange of B, C, O, Al, Si, S, F and Cl Passing through Thin Carbon Foils at Low Energies: Formation of Negative Ions*, Nucl. Instruments Methods Phys. Res. Sect. B Beam Interact. with Mater. Atoms **103**, 111 (1995).
- [52] E. Ntemou, R. Holeňák, and D. Primetzhofer, *Energy Deposition by H and He Ions at KeV Energies in Self-Supporting, Single Crystalline SiC Foils*, Radiat. Phys. Chem. **194**, 110033 (2022).
- [53] M. K. Linnarsson, A. Hallén, J. Åström, D. Primetzhofer, S. Legendre, and G. Possnert, *New Beam Line for Time-of-Flight Medium Energy Ion Scattering with Large Area Position Sensitive*

- Detector*, Rev. Sci. Instrum. **83**, 095107 (2012).
- [54] M. A. Sortica, M. K. Linnarsson, D. Wessman, S. Lohmann, and D. Primetzhofer, *A Versatile Time-of-Flight Medium-Energy Ion Scattering Setup Using Multiple Delay-Line Detectors*, Nucl. Instruments Methods Phys. Res. Sect. B Beam Interact. with Mater. Atoms **463**, 16 (2020).
- [55] See <https://www.norcada.com/products/silicon-membranes>, (unpublished).
- [56] R. Holeňák, S. Lohmann, and D. Primetzhofer, *Sensitive Multi-Element Profiling with High Depth Resolution Enabled by Time-of-Flight Recoil Detection in Transmission Using Pulsed KeV Ion Beams*, Vacuum **204**, 111343 (2022).
- [57] M. Bianconi, G. . Bentini, R. Lotti, and R. Nipoti, *Charge States Distribution of 0.16–3.3 MeV He Ions Transmitted through Silicon*, Nucl. Instruments Methods Phys. Res. Sect. B Beam Interact. with Mater. Atoms **193**, 66 (2002).
- [58] R. Holeňák, S. Lohmann, and D. Primetzhofer, *Contrast Modes in a 3D Ion Transmission Approach at KeV Energies*, Ultramicroscopy **217**, 113051 (2020).
- [59] A. Bürgi, M. Oetliker, P. Bochsler, J. Geiss, and M. A. Coplan, *Charge Exchange of Low-energy Ions in Thin Carbon Foils*, J. Appl. Phys. **68**, 2547 (1990).
- [60] J. A. Phillips, *Charge Equilibrium Ratios for Hydrogen Ions from Solids*, Phys. Rev. **97**, 404 (1955).
- [61] L. C. A. van den Oetelaar, S. N. Mikhailov, and H. H. Brongersma, *Mechanism of Neutralization in Low-Energy He⁺ Ion Scattering from Carbide and Graphitic Carbon Species on Rhenium*, Nucl. Instruments Methods Phys. Res. Sect. B Beam Interact. with Mater. Atoms **85**, 420 (1994).
- [62] S. Průša et al., *Highly Sensitive Detection of Surface and Intercalated Impurities in Graphene by LEIS*, Langmuir **31**, 9628 (2015).
- [63] Q. C. Kessel, M. P. McCaughey, and E. Everhart, *Coincidence Measurements of Ne⁺⁺-Ne Collisions*, Phys. Rev. **153**, 57 (1967).
- [64] A. N. Zinoviev, P. Y. Babenko, and A. P. Shergin, *Formation and Decay of Autoionization States as the Main Inelastic Energy Loss Mechanism in KeV Atomic Collisions*, J. Exp. Theor. Phys. **136**, 662 (2023).
- [65] R. Souda, M. Aono, C. Oshima, S. Otani, and Y. Ishizawa, *Mechanism of Electron Exchange between Low Energy He⁺ and Solid Surfaces*, Surf. Sci. **150**, L59 (1985).
- [66] H. Brongersma, M. Draxler, M. de Ridder, and P. Bauer, *Surface Composition Analysis by Low-Energy Ion Scattering*, Surf. Sci. Rep. **62**, 63 (2007).
- [67] R. Holeňák, E. Ntemou, S. Lohmann, M. Linnarsson, and D. Primetzhofer, *Assessing Trajectory-Dependent Electronic Energy Loss of KeV Ions by a Binary Collision Approximation Code*, Phys. Rev. Appl. **21**, 024048 (2024).

- [68] G. Schiwietz and P. L. Grande, *Unitary Convolution Approximation for the Impact-Parameter Dependent Electronic Energy Loss*, Nucl. Instruments Methods Phys. Res. Sect. B Beam Interact. with Mater. Atoms **153**, 1 (1999).
- [69] G. Schiwietz and P. L. Grande, *Convolution Approximation for Swift Particles (CasP)*, www.casp-program.org.
- [70] S. Tsuneyuki and M. Tsukada, *Theory of the Reionization Process Observed in Low-Energy He⁺ - Surface Scattering*, Phys. Rev. B **34**, 5758 (1986).
- [71] A. N. Zinoviev, P. Y. Babenko, D. S. Meluzova, and A. P. Shergin, *Excitation of Autoionization States and Electronic Stopping Powers at Collisions of Slow Ions with a Solid*, JETP Lett. **108**, 633 (2018).
- [72] R. Souda and M. Aono, *Interactions of Low-Energy He⁺, He⁰, and He* with Solid Surfaces*, Nucl. Inst. Methods Phys. Res. B **15**, 114 (1986).
- [73] P. L. Grande and G. Schiwietz, *Impact-Parameter Dependence of the Electronic Energy Loss of Fast Ions*, Phys. Rev. A **58**, 3796 (1998).
- [74] A. Hentz, G. S. Parkinson, P. D. Quinn, M. A. Muñoz-Márquez, D. P. Woodruff, P. L. Grande, G. Schiwietz, P. Bailey, and T. C. Q. Noakes, *Direct Observation and Theory of Trajectory-Dependent Electronic Energy Losses in Medium-Energy Ion Scattering*, Phys. Rev. Lett. **102**, 109 (2009).
- [75] J. I. Juaristi, A. Arnau, P. M. Echenique, C. Auth, and H. Winter, *Charge State Dependence of the Energy Loss of Slow Ions in Metals*, Phys. Rev. Lett. **82**, 1048 (1999).
- [76] V. V. Afrosimov, Y. S. Gordeev, A. M. Polyanskii, and A. P. Shergin, *Inelastic Energy Loss and Ionization in Excitation of Outer and Inner Electronic Shells During Atomic Collisions*, Sov. Phys. JETP **36**, 799 (1973).
- [77] K. Taulbjerg, B. Fastrup, and E. Laegsgaard, *Heavy-Ion-Induced X-Ray Production in Solids*, Phys. Rev. A **8**, 1814 (1973).
- [78] P. Riccardi and C. A. Dukes, *Excitation of the Triplet 2p⁴(3P)3s² Autoionizing State of Neon by Molecular Orbital Electron Promotion at Solid Surfaces*, Chem. Phys. Lett. **798**, 139610 (2022).